JJEES

JJEES (2026) 17 (2): 223-235
ISSN 1995-6681

Jordan Journal of Earth and Environmental Sciences

Identification of Social and Environmental Hotspots to Flood Risk on Cat Ba Island, Northern Vietnam

Phan Thi Mai Hoa[1, 2], Nguyen Quoc Phi[1*] and Nguyen Thi Cuc[1]

[1] Hanoi University of Mining and Geology, Hanoi, Vietnam
[2] Graduate University of Science and Technology, Vietnam Academy of Science and Technology, Vietnam

Received on 23 August 2025; Accepted on 1 December 2025

Abstract

This study identifies social and environmental hotspots associated with flood risk on Cat Ba Island, a climate-sensitive coastal region in Northern Vietnam. A spatial flood risk framework was developed by integrating the Analytic Hierarchy Process (AHP) with Geographic Information System (GIS) based Spatial Multi-Criteria Analysis (SMCA). Fourteen indicators representing terrain, hydrology, land use, and socio-demographics were standardized and weighted, with the AHP Consistency Ratio (CR = 0.04) confirming acceptable internal coherence. A Sentinel-1 SAR flood inventory from September 2024 was used for validation, showing a close match between the modeled risk zones and the observed inundation. Nearly all flooding (99.6%) occurred within the moderate-to-very high risk classes, while the low-risk zone experienced almost no inundation. Low-lying coastal areas, including Cat Ba Town and southern Tran Chau, emerge as the main hotspots due to dense settlement and limited drainage. Forested uplands show higher resilience. This study delivers the first empirically validated, high-resolution hotspot map for Cat Ba. It provides a clear, transferable framework to support climate adaptation and land-use planning in vulnerable island settings.

Keywords: *Analytic Hierarchy Process; Cat Ba Island; flood risk; Geographic Information System; social–environmental vulnerability.*

1. Introduction

Climate change poses profound threats to sustainable development globally, particularly through increasing flood risks that disproportionately affect coastal and island regions (Vousdoukas et al., 2023). Among these, small islands are considered highly vulnerable due to their low-lying topography, limited adaptive capacity, and exposure to sea-level rise, storm surges, and coastal erosion (Parmesan et al., 2022). In Southeast Asia, Vietnam is widely recognized as one of the most climate-exposed countries, with flood hazards threatening infrastructure, livelihoods, and economic resilience in both urban and rural areas (Boateng, 2012; Tuyet Hanh et al., 2020).

Cat Ba Island, the largest landmass in its archipelago and designated as a UNESCO Biosphere Reserve, represents a clear example of such vulnerability. Intensified flood events, resulting from rising sea levels, saltwater intrusion, and increasingly frequent typhoons, are placing increasing stress on critical infrastructure, including coastal roads and embankments, while directly impacting fisheries, tourism, and community well-being (Giang & Khanal, 2024).

Similar trends have been reported in other rapidly urbanizing settings, where increasing impermeable surfaces and limited drainage worsen flood impacts. (Oroud, 2025) shows that land-cover change in Amman has intensified runoff and concentrated flooding in low-lying districts. These conditions mirror what is now emerging on Cat Ba, where rapid tourism-driven expansion and inadequate drainage are increasing local flood susceptibility.

While significant attention has been given to physical exposure and hazard mapping, social vulnerability remains underexplored yet critical to climate risk. Socioeconomic conditions, such as high population density, limited access to services, and dependence on climate-sensitive livelihoods, can significantly limit communities' adaptive capacities (Cutter et al., 2012; Mai & Truong, 2022). In Vietnam, empirical studies indicate that combined pressures from flooding and salinization have intensified livelihood disruptions, triggered out-migration, and further deepened existing inequalities (Ta & Linh, 2024).

Although Vietnam's vulnerability to climate change has been widely acknowledged, most existing assessments focus on large-scale or provincial levels, lacking spatial granularity and place-specific insights. In particular, there remains a critical knowledge gap regarding fine-scale social vulnerability assessments for small islands such as Cat Ba, where localized socio-demographic characteristics and infrastructure limitations can substantially influence risk exposure (Dao & Dao, 2024; Van Phong et al., 2023).

This gap reflects broader global trends. Recent literature reviews have consistently identified enduring limitations in vulnerability assessments, particularly the insufficient incorporation of socioeconomic variables, the limited representation of localized contexts, and the lack of rigorous validation procedures (De Sherbinin et al., 2019). While an increasing number of studies have adopted integrated GIS-based frameworks, such as those utilizing AHP-based vulnerability assessments in Bangladesh (Ha-Mim &

* Corresponding author e-mail: nguyenquocphi@humg.edu.vn

Hossain, 2022), PCA combined with AHP models in Florida, USA (Xie & Meng, 2023), and multi-hazard mapping efforts in Romania (Ajtai et al., 2023; Chelariu et al., 2024). Most of these applications remain focused on urban or mainland regions. As a result, they seldom capture the compounded nature of social and environmental vulnerabilities in island communities.

National and regional vulnerability assessments are typically conducted at coarse spatial resolutions and depend on highly aggregated indices, which limit their relevance for local-scale adaptation. Existing reviews also note that most mapping efforts remain heavily oriented toward biophysical indicators, with only modest incorporation of social dimensions and very limited empirical validation against observed hazard impacts (Birkmann et al., 2022; Bukvic et al., 2020; De Sherbinin et al., 2019; Yarveysi et al., 2023). Against this backdrop, a fine-scale, empirically validated social–environmental vulnerability assessment for Cat Ba Island provides a useful complement to existing national and regional products.

Addressing this research gap, the present study applies a GIS-based Spatial Multi-Criteria Analysis (SMCA), integrated with the Analytic Hierarchy Process (AHP) to assess social vulnerability to flooding on Cat Ba Island. This integrated approach allows the combination of both environmental and socioeconomic indicators into a transparent, structured decision-making framework that is intuitive and adaptable to data-sparse environments. While advanced methods, such as machine learning, offer strong predictive performance, they often function as opaque "black boxes" that are difficult for local planners to interpret or adapt (De Sherbinin et al., 2019; Rudin, 2019; Uddameri & Hernandez, 2025). In contrast, the Analytic Hierarchy Process (AHP) provides a structured, transparent, and participatory framework that enables expert input and traceability, especially in data-scarce contexts (Ajtai et al., 2023). Accordingly, this study aims to (i) construct social and environmental hotspots to flood risk for Cat Ba Island using an integrated AHP and SMCA approach and (ii) validate its predictive performance using flood observations derived from Sentinel-1 Synthetic Aperture Radar (SAR) imagery. The findings are intended to support localized climate adaptation, risk reduction, and socially inclusive spatial planning in small island environments.

2. Study area

This study focuses on Cat Ba Island, the largest landmass in the Cat Ba Archipelago, located off the northeastern coast of Vietnam in Hai Phong Province, situated between 106°54′20″–107°07′20″E and 20°42′40″–20°52′40″N. Cat Ba Island and its surrounding islets cover a total area of approximately 173 km², as shown in Figure 1. The archipelago has a mean elevation of approximately 200 m above sea level, reflecting a dissected karst landscape dominated by steep ridges and narrow valleys (Van Quan et al., 2010). Demographically, Cat Ba Island has around 18,000–19,000 permanent residents. Recognized as a UNESCO Biosphere Reserve since 2004, the island encompasses diverse landscapes including karst limestone formations, tropical forests, and low-lying coastal zones (Hue et al., 2024). Its socioeconomic profile is shaped by a rapidly expanding tourism industry, small-scale aquaculture, and dispersed residential communities, many of which are situated in areas increasingly exposed to flood hazards (Hoang & Truong, 2023). Intensifying typhoons, shoreline erosion, and saltwater intrusion have placed mounting pressure on infrastructure systems and local livelihoods (Maliva, 2021), underscoring Cat Ba's significance as a representative site for assessing the intersection of climate-related social and environmental vulnerabilities.

Historical disaster records indicate that Cat Ba has experienced recurrent inundation in recent years. Typhoon Yagi in 2024 produced extensive flooding across Cat Ba Town and surrounding low-lying areas, disrupting transport and coastal infrastructure (VnExpress, 2024). More recently, prolonged rainfall in September 2025 caused additional inundation in Xuan Dam, Viet Hai, Cat Ba Town and Phu Long, with flood depths ranging from approximately 0.2 to 0.5 m and lasting for 1–3 hours (Newspaper, 2025). Such recurring events highlight the urgency of identifying social and environmental hotspots of flood risk on Cat Ba Island to inform adaptive planning and risk-reduction strategies.

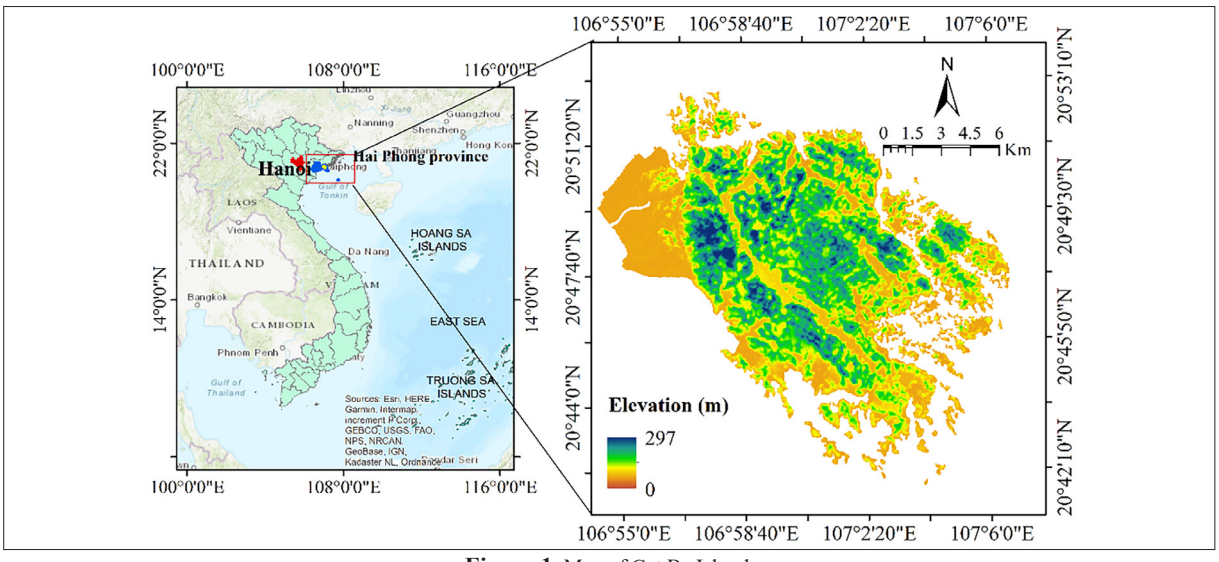

Figure 1. Map of Cat Ba Island.

3. Methodology

3.1. Materials

Fourteen spatial criteria were selected to represent key environmental and social factors influencing climate-related flood risk on Cat Ba Island. The criteria encompass terrain (elevation, slope), hydrological exposure (distance to rivers, rainfall, drainage density, stream power index, topographic wetness index), land cover (land use/land cover, NDVI, NDWI), and social exposure (population and building density, distance to services). Table 1 summarizes selected flood vulnerability indicators, including LULC, river proximity, slope, elevation, rainfall, NDWI, TWI, SPI, and NDVI, as well as their classification thresholds, data sources, and influence on vulnerability, based on expert knowledge and literature relevant to regional flooding.

Prior to analysis, each layer was standardized to a uniform vulnerability scale, ranging from 1 to 5, to ensure comparability, with higher scores indicating greater vulnerability (Table 1 and Figure 2). Direct factors, such as population density, were scored positively (higher values representing higher vulnerability), while inverse factors, such as distance to health facilities, were reverse-scored (greater distance indicating higher vulnerability). For example, elevation was reclassified so that low-lying coastal areas (<5 m) received very high vulnerability scores. In contrast, higher terrain was assigned lower scores, consistent with coastal flood risk assessments (Khan et al., 2025). Definitions of influence direction were determined to maintain consistency across criteria.

All indicators were processed and standardized on a 30-meter spatial resolution grid covering the entire Cat Ba Island study area. The resolution was selected to align with the spatial resolution of the primary base datasets, including the SRTM 30 m Digital Elevation Model, Sentinel-2 MSI (10–30 m), and the Google Dynamic World V1 (10 m resampled to 30 m). Below is a summary of the indicators used:

Land Use/Land Cover (LULC): Areas dominated by urban or impervious surfaces tend to have increased runoff and higher flood risk, whereas regions with natural vegetation or wetlands can enhance infiltration and mitigate flooding (Khodaei et al., 2025). We classified LULC types so that built-up or bare land areas receive higher vulnerability scores, while forested or wetland areas receive lower scores.

Distance to Rivers (DRi): Proximity to rivers elevates exposure to fluvial flooding (e.g., overbank flows and backwater effects). Locations closer to river channels are thus considered more vulnerable, as even moderate rain events can lead to flooding in adjacent lowlands (Khan et al., 2025; Miranda et al., 2023).

Slope: Flat or low-slope areas allow water to accumulate and stagnate, making them more prone to inundation, whereas steep slopes facilitate faster runoff and are generally less flood-prone (Khan et al., 2025; Tariq et al., 2022). We assigned higher vulnerability scores to gentler slopes.

Elevation: Low-elevation zones (especially <5 m above sea level) are highly susceptible to coastal flooding and storm surges, while higher-elevation areas are less exposed. Accordingly, lower elevations were scored as more vulnerable.

Rainfall (Annual): Regions with higher precipitation totals are likely to experience greater runoff volumes and flood frequencies. Areas on Cat Ba with higher long-term average rainfall were thus scored as having higher flood vulnerability. The mean rainfall for 2024 was derived through interpolation in ArcGIS.

Normalized Difference Water Index (NDWI): NDWI is a remote sensing index that emphasizes the presence of surface water and soil saturation by contrasting near-infrared and shortwave infrared reflectance. High NDWI values indicate the presence of standing water bodies or marshy conditions, signaling existing flood-prone or waterlogged areas (Abijith et al., 2025; Ji et al., 2009; Konapala et al., 2021). Areas with persistently high NDWI were considered more vulnerable.

Topographic Wetness Index (TWI): TWI models the potential for soil saturation and water accumulation based on terrain shape. Higher TWI values correspond to locations where water naturally converges and accumulates (e.g., valleys and depressions), thereby correlating with increased flood susceptibility (Abijith et al., 2025; Adnyana & Wiguna, 2025).

Stream Power Index (SPI): SPI measures the erosive power of flowing water and is related to slope and drainage area. Lower SPI values often identify low-gradient plains or wide valleys where water loses energy and can pond or overflow, increasing flood risk (Abijith et al., 2025; Kocsis et al., 2022). In our context, areas with low SPI (indicative of low slope and high potential water accumulation) were marked as more vulnerable.

Normalized Difference Vegetation Index (NDVI): NDVI quantifies vegetation density by measuring the difference in reflectance between near-infrared and visible red wavelengths. Areas with dense vegetation cover (high NDVI) can intercept rainfall, promote infiltration, and stabilize soils, thereby reducing runoff and flood severity. Conversely, sparsely vegetated or barren areas (low NDVI) exacerbate flood vulnerability due to higher runoff (Khan et al., 2025). Thus, lower NDVI areas were scored higher for vulnerability.

Drainage Density (DD): Drainage density represents the total length of streams and rivers per unit area. Regions with a high density of drainage channels may experience more concentrated runoff and potentially more severe flooding within those channels (Abijith et al., 2025; Rautela et al., 2023; Tetteh et al., 2024). High drainage density can be a double-edged factor: it indicates efficient water removal, but also means many areas are near a watercourse. In our scoring, extremely high drainage density areas were treated carefully, often in conjunction

with proximity to channels (as represented by the Distance to Rivers criterion).

Population Density (PopD): Higher population density indicates that more people and assets are exposed within a given area, raising the potential human impact of any flood event (Ibrahim et al., 2024). Densely populated neighborhoods on Cat Ba were thus given higher vulnerability scores, reflecting the higher stakes in those areas.

Building Density (BD): A high concentration of buildings often correlates with more impervious surfaces and reduced infiltration, which can increase runoff and flood intensity. Moreover, a greater number of structures means more property at risk. Areas with high building density were marked as more vulnerable to flooding (Son et al., 2023).

Distance to Nearest School: Schools and educational facilities often serve as emergency shelters or coordination centers during disasters. Communities located far from a school may have reduced access to safe shelters or organized relief in a flood event. Therefore, a greater distance from the nearest school was interpreted as higher social vulnerability (Isia et al., 2023).

Distance to Nearest Health Center: Access to healthcare is crucial during and after flood emergencies for treating injuries and illnesses. Communities that are farther from clinics or hospitals experience delays in receiving medical care. Thus, a longer distance to the nearest health center contributes to higher vulnerability (Zhran et al., 2024).

Each of these criteria was classified into five ordinal vulnerability classes (1-5) based on value ranges informed by previous studies and local expert consultations. This classification approach was iteratively refined to ensure that the resulting criteria maps aligned with local knowledge of past flood impacts, thereby increasing the reliability of our integrated assessment.

To quantify actual flood extents and validate the predictive accuracy of the composite flood risk zones, a flood inventory was generated using time-series Sentinel-1 SAR imagery. The change detection method was applied by calculating the backscatter difference between pre-flood and post-flood acquisitions, leveraging the sensitivity of SAR signals to surface water (Konapala et al., 2021). A threshold-based classification was then employed to isolate flooded pixels, with calibration based on field knowledge and visual interpretation of high-resolution optical imagery.

Table 1. Criteria for Vulnerability Assessment.

No.	Data	Classification level					Data sources
		Very low	Low	Moderate	High	Very high	
1	Elevation	0-30	30-74	74-120	120-169	169-297	Topographic maps (1:10.000 scale)
2	Slope	0-8.2	8.2-17.2	17.2-26.1	26.1-36.7	36.7-74	Topographic maps (1:10.000 scale)
3	Distance to rivers (DRi)	0-1203	1203-2203	2203-3159	3159-4270	4270-7080	OpenStreetMap (OSM)
4	Drainage density (DD)	0-0.08	0.08-0.3	0.3-0.6	0.6-0.9	0.9-1.5	OpenStreetMap (OSM)
5	Rainfall (annual)	231-260	260-277	277-290	290-302	302-325	CHIRPS daily rainfall dataset ("UCSBCHG/CHIRPS/DAILY")
6	NDVI	-0.25 -0.01	0.01-0.22	0.22-0.38	0.38-0.49	0.49-0.78	Landsat 8 imagery NDVI = (band 5- band4)/(band5+band4)
7	NDWI	-0.70–-0.44	-0.44–-0.33	-0.33–-0.16	-0.16-0.05	0.05-0.35	Sentinel-2 imagery of 2024
8	TWI	-4.9–-2.9	-2.9–-1.3	-1.3-0.9	0.9-3.8	3.8-10.5	Topographic maps (1:10.000 scale)
9	SPI	0-0.25	0.25-1	1-2.2	2.2-4.8	4.8-12.8	Topographic maps (1:10.000 scale)
10	Land use/land cover (LULC) - 2021	0-10	10-40	40-60	60-80	80-95	Google Dynamic World V1 (Sentinel-2)
11	Population density	2.5	2.5-4.9	4.9-41	41.66	66-215	National census (2019)
12	Building density	0-1431	1431-2483	2483-3535	3535-4821	4821-7451	Google Earth + Field Verification
13	Distance to nearest school	0-2918	2918-5551	5551-7955	7955-10244	10244-14595	Google Earth + Field Verification
14	Distance to nearest health center	0-76	76-252	252-487	487-803	803-1107	Google Earth + Field Verification

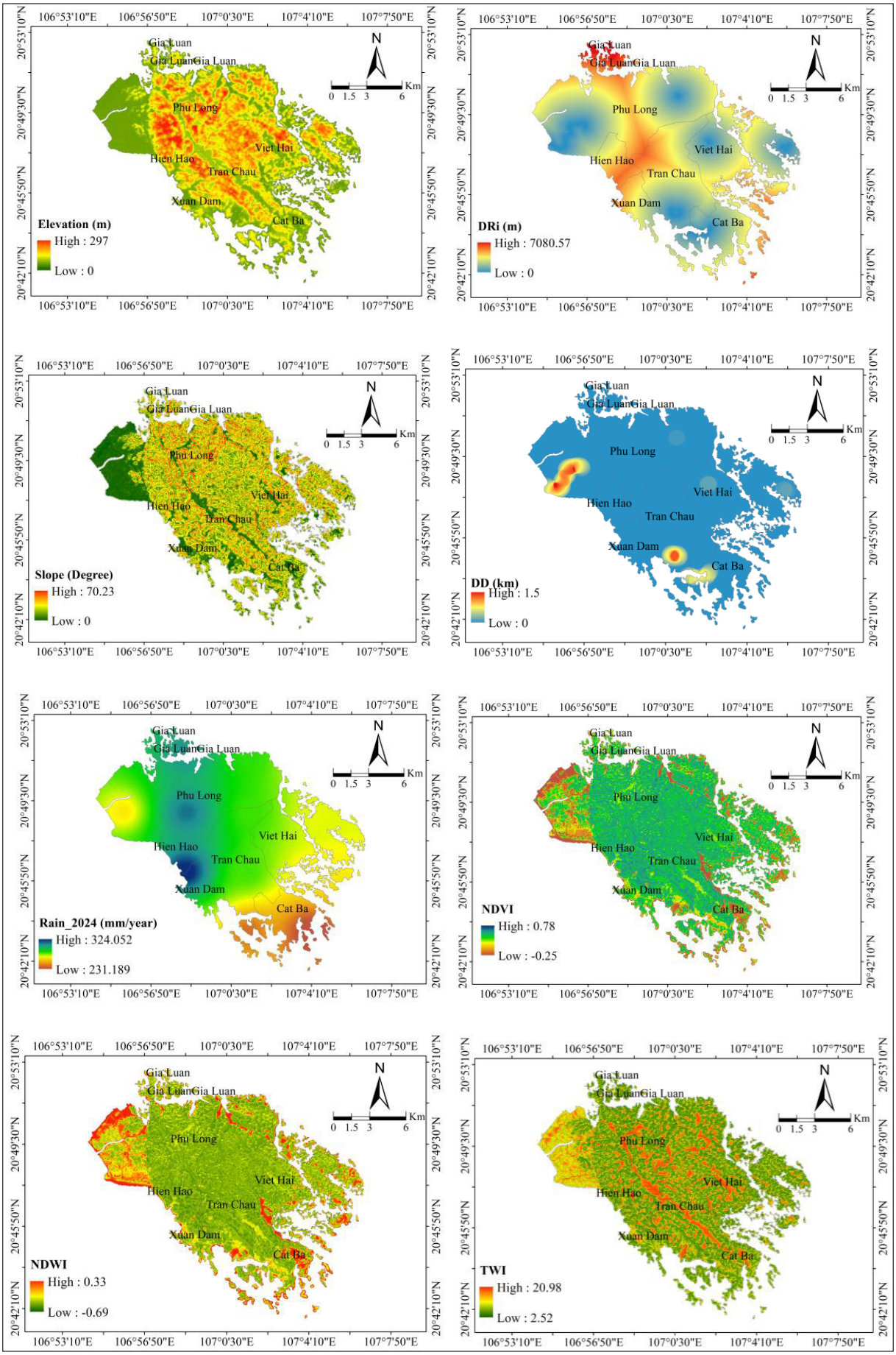

Figure 2. Input layers for flood vulnerability assessment and Sentinel-1 inundation map (Sept 2024).

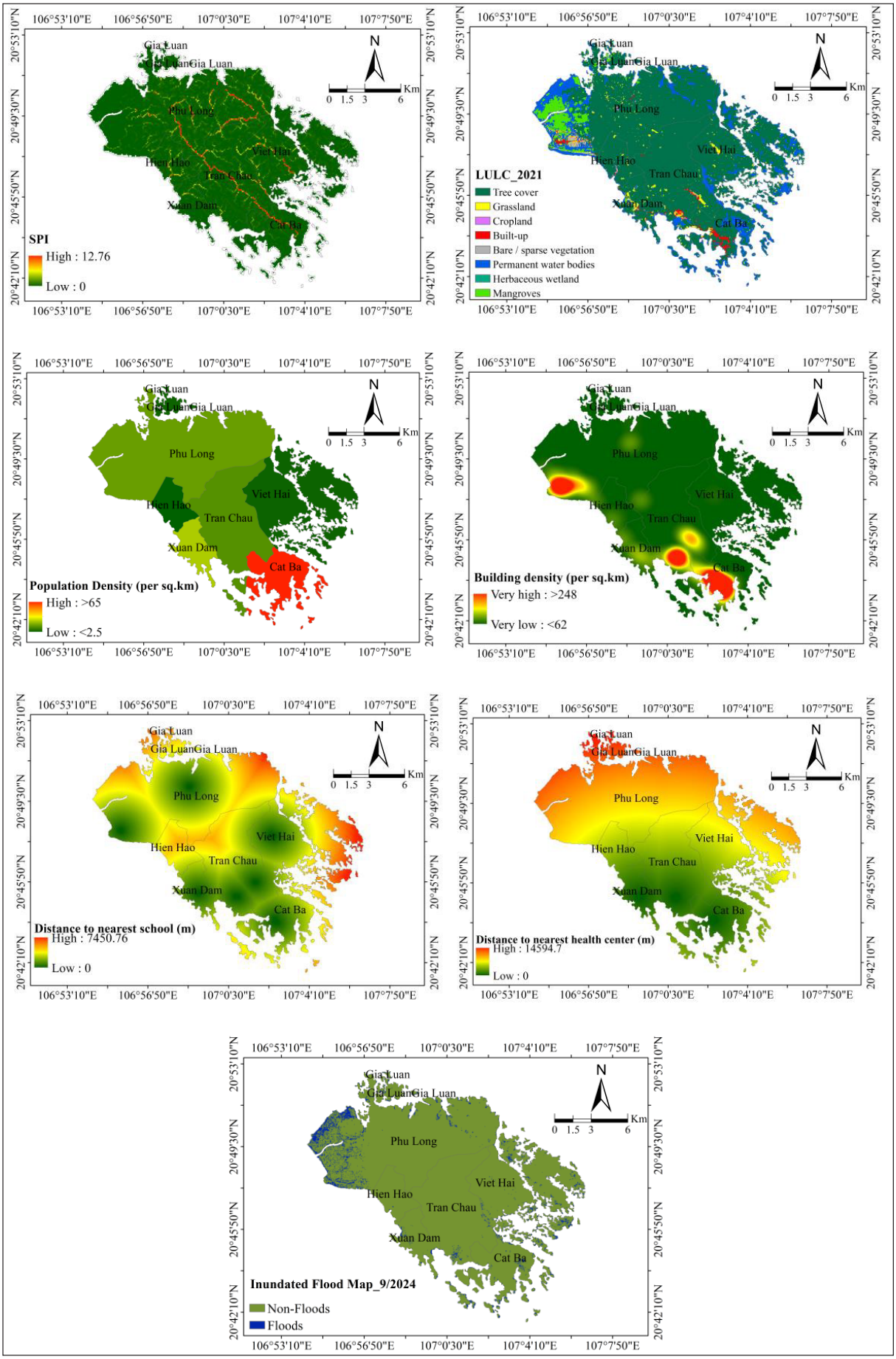

Continuing from Figure 2. Input layers for flood vulnerability assessment and Sentinel-1 inundation map (Sept 2024).

3.2. Method

To integrate the selected criteria and produce a composite flood vulnerability map, this study implemented a GIS-based Spatial Multi-Criteria Analysis (SMCA) combined with the Analytic Hierarchy Process (AHP) for factor weighting. The methodological workflow consisted of four key steps: data preprocessing, indicator standardization, expert-based weighting using AHP, and GIS-based weighted overlay analysis (Figure 3). The AHP method was selected for its capacity to systematically incorporate expert knowledge and local context into the evaluation model, which is particularly advantageous for place-specific assessment (Saaty, 1980). Unlike purely statistical techniques, AHP employs a structured pairwise comparison framework that captures expert judgments on the relative importance of factors, effectively reflecting local realities, such as prioritizing population density over minor topographic variations when assessing flood risk. The widespread application of AHP in climate vulnerability studies stems from its transparency and flexibility in integrating both qualitative and quantitative data (Al-Sababhah, 2023; Bharwani et al., 2013; Udie et al., 2018). Pairwise comparisons in this study were informed by a panel of local experts, including community planners and disaster risk management officials, to ensure alignment of the derived weights with practical experiences with climate hazards in the Cat Ba context.

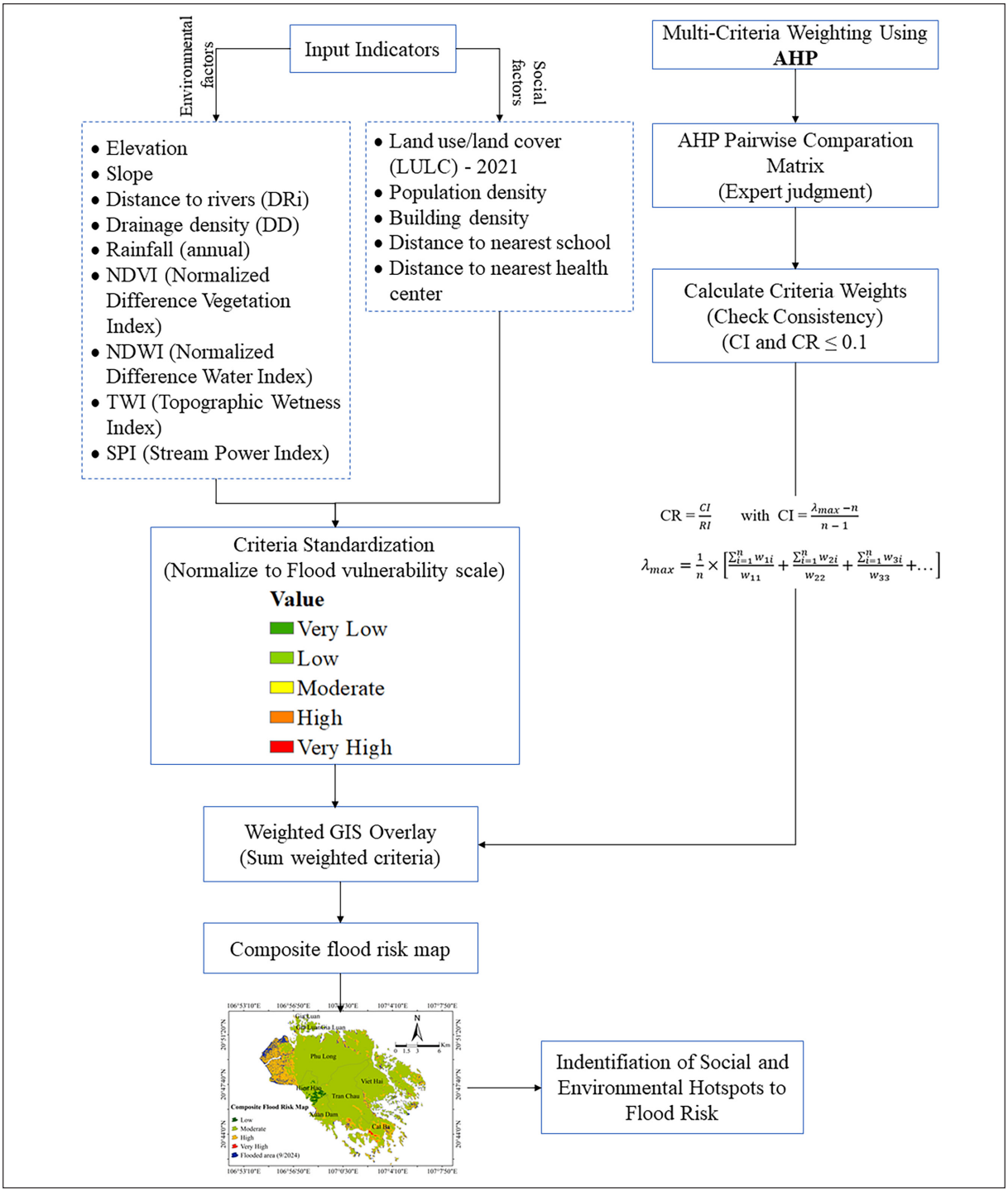

Figure 3. Workflow of the proposed approach to the composite flood risk map.

The Analytic Hierarchy Process (AHP), a structured multi-criteria decision-making (MCDM) technique, was adopted to rank and weight environmental and social factors influencing vulnerability.

Pairwise comparisons were conducted using Saaty's 1–9 scale (Figure 4), where a score of 1 reflects equal importance and a score of 9 indicates a strong preference for one factor over another (Saaty, 1980). Evaluations from a panel of disaster management and environmental experts were used to complete the comparison matrix, and the principal eigenvector was calculated to obtain normalized weights, representing the relative contribution of each criterion to overall vulnerability.

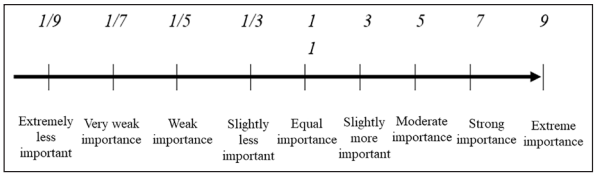

Figure 4. Standard AHP Intensity Scale (Saaty, 1980).

Consistency of expert judgments was verified by calculating the Consistency Ratio (CR), defined in Eq. (1). A CR below the recommended threshold of 0.1 indicated acceptable consistency, thereby ensuring the reliability of the derived weights (Saaty, 1980). In the present analysis, all matrices met this consistency requirement.

$$\mathrm{CR} = \frac{CI}{RI} \tag{1}$$

$$\text{with } \mathrm{CI} = \frac{\lambda_{max} - n}{n - 1} \tag{2}$$

$$\lambda_{max} = \frac{1}{n} \times \left[\frac{\sum_{i=1}^{n} w_{1i}}{w_{11}} + \frac{\sum_{i=1}^{n} w_{2i}}{w_{22}} + \frac{\sum_{i=1}^{n} w_{3i}}{w_{33}} + \ldots \right] \tag{3}$$

where λmax is the principal eigenvalue of the comparison matrix, and nnn is the number of criteria. The CI measures the degree to which the judgments deviate from complete consistency.

The Random Index (RI), reflecting the average consistency of a randomly generated reciprocal matrix, is adopted from Saaty's guidelines (1980). For a comparison matrix of order n = 14, the corresponding RI value is 1.57 (Alonso & Lamata, 2006). Subsequently, Geographic Information System (GIS) techniques were employed to produce a composite social vulnerability map. Each spatial data layer representing a criterion was reclassified and multiplied by its corresponding AHP-derived weight. The weighted layers were then aggregated through linear combination to generate a continuous vulnerability index surface.

To support spatial interpretation, the continuous vulnerability surface was categorized into four discrete classes: Low, Moderate, High, and Very High vulnerability. Classification thresholds were determined using the Jenks Natural Breaks optimization method, which minimizes within-class variance and maximizes between-class differences (Komolafe et al., 2020). This method was chosen for its suitability in environmental and spatial data classification, particularly when values are not uniformly distributed. The resulting vulnerability classes reflect the relative severity of flood susceptibility across the study area and were validated against expert knowledge and observed inundation patterns.

The final classified flood vulnerability map was then overlaid with the Sentinel-1–derived flood inventory to assess predictive accuracy. This validation step involved spatial cross-tabulation between predicted vulnerability zones and actual flood extents, allowing for quantitative evaluation of model performance (Shivhare et al., 2024). The high degree of spatial alignment between predicted high-vulnerability zones and observed flooded areas provided empirical support for the reliability of the composite risk assessment.

4. Results and Discussion

4.1. Spatial Indicators of Flood Vulnerability

The spatial pattern of flood-related vulnerability on Cat Ba Island reflects the combined influence of environmental exposure, surface conditions, and settlement characteristics. High-vulnerability zones are concentrated in low-lying coastal centers such as Cat Ba Town and Xuan Dam, where dense construction, limited open space, and constrained drainage create conditions favorable for recurrent inundation. Conversely, upland communes such as Viet Hai and Gia Luan exhibit lower susceptibility due to intact vegetation and steeper terrain that facilitate runoff and enhance natural infiltration.

The results derived from the pairwise comparison matrix (Table 2) and the normalized weights (Table 3) show that built-environment and demographic indicators dominate the weighting structure, with population density, building density, and land-use characteristics ranking among the most influential criteria in the AHP evaluation. Population density (24.27%) and building density (18.12%) were the strongest contributors, followed by land use/land cover (12.80%) and NDWI (9.39%) (Table 3), indicating the role of urban expansion, impervious surfaces, and surface saturation in amplifying flood impacts. These findings align with previous work highlighting population pressure and urban form as central determinants of vulnerability in hazard-prone settings (Balaian et al., 2024; Cutter et al., 2012; Ma & Mostafavi, 2024). Hydrological indicators, such as proximity to rivers (6.55%) and drainage density (5.22%), exert secondary influence but remain important for explaining runoff concentration on valley floors and in constrained drainage corridors.

The spatial interaction between these factors produces a clear coastal–upland divide. Urbanized southern centers with extensive impervious cover show strong correspondence with high NDWI values and limited drainage pathways, resulting in concentrated flood hotspots. This pattern is also evident in Phu Quoc (Dao & Dao, 2024) and other tourism-driven island destinations (Du et al., 2015), where similar combinations of dense built-up areas and constrained drainage consistently amplify flood risk. Although rivers normally function as natural drainage corridors, poorly designed or undersized embankments can impede flow and intensify localized flooding, a pattern also observed in other urbanized watersheds (Zakir, 2024).

In contrast, forested uplands retain greater resilience due to higher vegetation cover and terrain gradients that limit water accumulation (Janzen et al., 2024; Justine & Seenath, 2025) on vegetation-mediated hazard mitigation.

Access to essential services, as reflected in the distance to schools (2.86%) and health centers (2.68%), further differentiates communities, highlighting areas where isolation may intensify the impacts of extreme events (Alabbad & Demir, 2025; Hamza et al., 2021).

Table 2. Pairwise comparison matrix.

Factors	Elevation	Slope	Distance to rivers	Drainage density	Rainfall (annual)	NDVI	NDWI	TWI	SPI	LULC	Population density	Building density	Distance to nearest school	Distance to nearest health center
Elevation	1	1	0.3	0.3	0.5	0.5	0.2	0.5	1	0.14	0.1	0.1	2	1
Slope	1	1	0.3	0.3	0.5	0.5	0.2	0.5	1	0.1	0.1	0.1	2	2
Distance to rivers	4	4	1	2	2	2	0.5	2	2	0.5	0.3	0.3	2	2
Drainage density	3	3	0.5	1	2	2	0.5	1	2	0.333	0.3	0.25	2	2
Rainfall (annual)	2	2	0.5	0.5	1	2	0.33	2	1	0.25	0.17	0.2	1	1
NDVI	2	2	0.5	0.5	0.5	1	0.3	2	2	0.25	0.14	0.20	1	1
NDWI	6	6	2	2	3	3	1	3	3	0.5	0.25	0.5	3	3
TWI	2	2	0.5	1	0.5	0.5	0.3	1	2	0.3	0.14	0.17	1	1
SPI	1	1	0.5	0.5	1.0	0.5	0.3	0.5	1	0.17	0.11	0.13	2	2
LULC	7	8	2	3	4.0	4	2	4	6	1	0.33	0.5	4	3
Population density	9	9	4	4	6	7	4	7	9	3	1	2	7	7
Building density	9	9	3	4	5	5	2	6	8	2	0.5	1	6	6
Distance to nearest school	0.5	0.5	0.5	0.5	1	1	0.3	1	1	0	0.1	0.2	1	2
Distance to nearest health center	1	0.5	0.5	0.5	1	1	0.3	1	1	0	0.1	0.2	0.5	1
SUM	48.5	49	16	20.17	28	30	12.33	31.5	39	9.10	3.65	5.83	34.5	34

Table 3. Normalization of matrix and final weights.

Factors	Elevation	Slope	Distance to rivers	Drainage density	Rainfall (annual)	NDVI	NDWI	TWI	SPI	LULC	Population density	Building density	Distance to nearest school	Distance to nearest health center	Weighted
Elevation	0.021	0.020	0.016	0.017	0.018	0.017	0.014	0.016	0.026	0.016	0.030	0.019	0.058	0.029	0.0225
Slope	0.021	0.020	0.016	0.017	0.018	0.017	0.014	0.016	0.026	0.014	0.030	0.019	0.058	0.059	0.0245
Distance to rivers	0.082	0.082	0.063	0.099	0.071	0.067	0.041	0.063	0.051	0.055	0.068	0.057	0.058	0.059	0.0655
Drainage density	0.062	0.061	0.031	0.050	0.071	0.067	0.041	0.032	0.051	0.037	0.068	0.043	0.058	0.059	0.0522
Rainfall (annual)	0.041	0.041	0.031	0.025	0.036	0.067	0.027	0.063	0.026	0.027	0.046	0.034	0.029	0.029	0.0373
NDVI	0.041	0.041	0.031	0.025	0.018	0.033	0.027	0.063	0.051	0.027	0.039	0.034	0.029	0.029	0.0350
NDWI	0.124	0.122	0.125	0.099	0.107	0.100	0.081	0.095	0.077	0.055	0.068	0.086	0.087	0.088	0.0939
TWI	0.041	0.041	0.031	0.050	0.018	0.017	0.027	0.032	0.051	0.027	0.039	0.029	0.029	0.029	0.0329
SPI	0.021	0.020	0.031	0.025	0.036	0.017	0.027	0.016	0.026	0.018	0.030	0.021	0.058	0.059	0.0289
LULC	0.144	0.163	0.125	0.149	0.143	0.133	0.162	0.127	0.154	0.110	0.091	0.086	0.116	0.088	0.1280
Population density	0.186	0.184	0.250	0.198	0.214	0.233	0.324	0.222	0.231	0.330	0.274	0.343	0.203	0.206	0.2427
Building density	0.186	0.184	0.188	0.198	0.179	0.167	0.162	0.190	0.205	0.220	0.137	0.172	0.174	0.176	0.1812
Distance to nearest school	0.010	0.010	0.031	0.025	0.036	0.033	0.027	0.032	0.013	0.027	0.039	0.029	0.029	0.059	0.0286
Distance to nearest health center	0.021	0.010	0.031	0.025	0.036	0.033	0.027	0.032	0.013	0.037	0.039	0.029	0.014	0.029	0.0268

Altogether, the results reveal a distinct spatial dichotomy: flood vulnerability clusters in urbanized, low-lying coastal zones, while forested upland areas exhibit lower susceptibility. This pattern reflects the interplay between built infrastructure, socioeconomic exposure, and natural buffering systems. And the AHP–SMCA framework effectively captures these spatial relationships and provides a robust basis for prioritizing climate-resilient planning on small islands.

4.2. Social-Environmental hotspots to flood risk on Cat Ba Island

This study underscores the value of integrating GIS-based Spatial Multi-Criteria Analysis (SMCA) with the Analytic Hierarchy Process (AHP) to assess flood-related environmental, social vulnerability at a fine spatial scale. The weighting of 14 indicators produced a consistency ratio (CR) of 0.04, well below the 0.1 threshold (Saaty, 1980), confirming the reliability of expert-based judgments. The AHP–SMCA framework proves especially suited to small island settings, offering a transparent and transferable tool for spatial risk diagnostics.

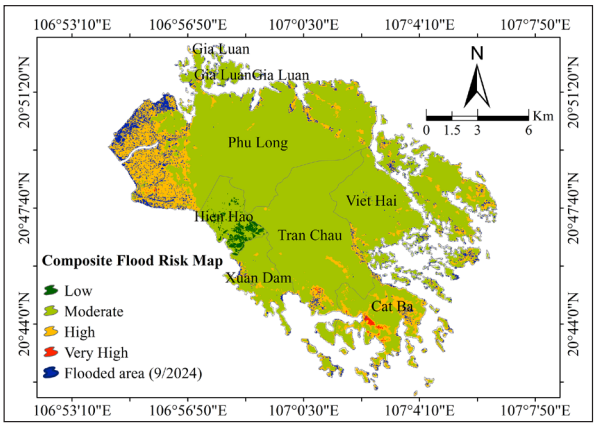

Figure 5. Composite Flood Risk Map of Cat Ba Island.

The comparison between the composite flood-risk map and the 2024 inundation footprint shows a strong correspondence in both magnitude and spatial pattern (Figure 5). Of the 172.85 km² study area, only 16.66 km² (9.6%) was flooded, and almost all of this inundation occurred within zones classified as moderate, high, or very high risk. The relationship between predicted risk zones and actual flood impacts becomes evident in Figure 6, where the extent of 2024 inundation is displayed alongside the area of each risk class. The low-risk class occupies just 0.06 km² (0.03% of the island) and contains only 0.00006 km² of flooding, confirming that areas mapped as low risk are effectively unaffected. Although the moderate-risk zone covers the largest share of the island (138.31 km²; 80%), it experienced only 5.91 km² of inundation (4.3% of its area). In contrast, the high-risk class (33.80 km²; 19.6%) contains 5.92 km² of flooding, accounting for 35.5% of the total inundation. The very-high-risk class shows the most pronounced contrast: although it occupies only 0.69 km² (0.4% of the island), the surrounding inundation associated with this class reaches 4.83 km², or nearly 29% of all observed flooding. These area ratios and the close spatial alignment show that flooded patches are concentrated mainly in low-lying coastal sectors classified as high or very high risk, whereas inland areas dominated by the moderate-risk class remain largely unaffected. Together, these patterns indicate that the composite flood-risk map effectively captures the principal flood-prone zones on Cat Ba Island.

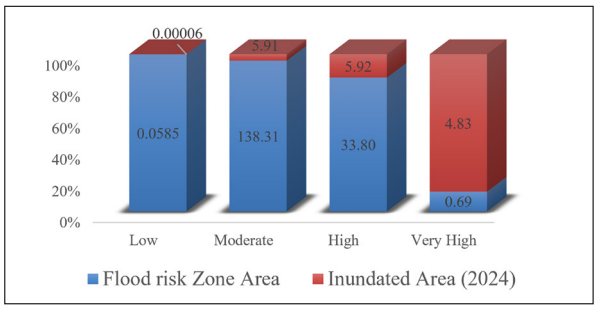

Figure 6. Discrepancy between flood risk zones and actual inundation (Sept 2024).

Several spatial hotspots aligned with the High and Moderate risk zones. In southern Tran Chau and Cat Ba town, high flood intensity was associated with low elevation, dense urbanization, and inadequate drainage systems. In Phu Long, both the ferry terminal area and western lowlands showed considerable exposure due to tidal backflow, estuarine influence, and functional infrastructure density. Meanwhile, southern Tran Chau, near Cat Ba town, displayed notable localized flooding patterns concentrated in natural depressions and valley floors, suggesting a combination of poor drainage and low-relief terrain.

By contrast, Hien Hao, which is located on the island's western flank, was predominantly classified as Very Low to Low flood risk, with minimal recorded inundation. This outcome can be attributed to several favorable physiographic and land cover characteristics. The area is dominated by elevated terrain, steep slopes, and dense vegetation, which facilitate rapid surface runoff and reduce water accumulation. Additionally, the absence of major urban infrastructure and minimal alteration of natural drainage patterns further mitigates the flood hazard in this sector. The contrast between Hien Hao and the southern lowland areas reinforces the role of topography, land use, and hydrological connectivity in defining localized flood risk.

Overall, these spatial patterns emphasize the need for targeted flood mitigation strategies that go beyond general zoning and address specific vulnerabilities in both densely developed and geomorphologically constrained areas of Cat Ba Island.

4.3. Discussion

The spatial distribution of social vulnerability on Cat Ba Island reveals a clear coastal-inland divide, carrying significant implications for both localized planning and broader theoretical discourse. High-vulnerability zones are primarily concentrated in low-lying, densely populated coastal communities (e.g., Cat Ba Town and Xuan Dam), whereas interior upland areas with intact forests and steeper terrain demonstrate markedly lower vulnerability. Figures 5 and 6 highlight that flood events in 2024 were largely confined to socially and environmentally vulnerable hotspots, thereby reinforcing the model's capacity to accurately delineate flood-prone zones on Cat Ba Island despite their

limited spatial extent. In essence, the GIS–AHP analysis not only pinpoints social–environmental hotspots of flood risk, but also empirically validates that elevated predicted vulnerability corresponds with a disproportionately high incidence of real-world flood impacts.

From a policy standpoint, this study provides a practical and spatially explicit framework for climate adaptation and spatial planning by identifying flood-prone social and environmental hotspots on Cat Ba Island. The results enable local authorities to prioritize high-risk zones such as Cat Ba Town and southern Tran Chau for targeted interventions such as drainage enhancement, climate-resilient infrastructure, and community-based preparedness strategies. Given the island's constrained evacuation capacity and infrastructure, strengthening adaptive capacity in urbanized coastal zones is especially urgent. Moreover, the findings underscore the need to regulate unplanned development in low-lying areas and to mainstream flood risk considerations into spatial planning processes. The overlay of flood data from 2024 further supports the critical protective role of upland forests and coastal mangroves, underscoring the value of nature-based solutions as cost-effective, complementary alternatives to conventional engineered defenses.

Beyond its practical applications, this study contributes to the theoretical understanding of flood vulnerability by illustrating how social and environmental factors interact to create concentrated risk in insular settings. On Cat Ba Island, high-exposure zones, which are characterized by dense populations, limited services, and poor drainage, closely align with areas of low elevation and intense land-use pressure. Together, these overlapping conditions give rise to well-defined social–environmental hotspots. This spatial overlap illustrates the compound nature of vulnerability, where socioeconomic stress and physical exposure reinforce each other. The contrast between flood-prone urban lowlands and more resilient upland areas highlights how vulnerability is highly place-specific and shaped by human–environment dynamics. By providing fine-scale, empirical evidence from a small island context, the study advances current frameworks by emphasizing the need for integrated approaches to climate risk that account for both social conditions and environmental constraints simultaneously.

The methodological contribution of this study lies in developing a transparent and replicable workflow that integrates AHP, GIS-based Spatial Multi-Criteria Analysis (SMCA), and Sentinel-1 SAR–derived flood data. The use of SAR imagery provided a robust validation layer, demonstrating that areas identified as highly vulnerable indeed corresponded with observed flood extents in 2024. By balancing expert-derived judgment with empirical satellite evidence, the approach ensures transparency and avoids the opacity of data-intensive "black box" models. Its reliance on open-access datasets and standard GIS techniques further enhances the transferability of the method to other small island settings facing similar constraints in monitoring capacity and planning resources. While the approach offers clear methodological and practical advantages, several limitations should be acknowledged to contextualize the findings and guide future research. Several methodological limitations warrant consideration. First, the use of 30-m resolution datasets may underrepresent micro-topographic depressions, drainage channels, and fine-scale urban structures that strongly influence local flood dynamics. Second, the AHP framework relies on expert judgment, which introduces a degree of subjectivity into the weighting process; although consistency checks were applied, the results may still vary depending on the composition and experience of the expert panel. Third, Sentinel-1 SAR imagery introduces potential uncertainty in steep or forested terrain, where layover, shadowing, and wet-surface backscatter can distort flood detection. Future work may address these limitations by incorporating higher-resolution elevation data, using multi-temporal SAR observations, and testing machine-learning classifiers. Such improvements would help enhance both the predictive accuracy and the broader applicability of the hotspot-based flood-risk framework.

5. Conclusion

This study demonstrates a practical and conceptually grounded approach for identifying social–environmental flood hotspots on Cat Ba Island by integrating expert-informed AHP weighting with spatial multi-criteria analysis. The framework advances current practice by linking social conditions with physical exposure in a single, transparent workflow that remains operational even in data-limited island environments. Validation with Sentinel-1 observations confirms that the model captures the spatial distribution of flood impacts, underscoring its suitability for risk screening and early-stage planning. More broadly, the approach offers a transferable tool for local governments seeking to prioritize adaptation measures, strengthen community preparedness, and safeguard natural buffers. Its emphasis on the combined social and environmental dimensions provides a useful direction for future climate-risk assessments on small islands, where tightly coupled human–environment dynamics shape vulnerability. Future work should build on this foundation by incorporating higher-resolution datasets and multi-event flood observations to enhance predictive robustness and support long-term climate adaptation strategies.

Acknowledgment

This research was funded and facilitated by the 2025 institutional science and technology project at Hanoi University of Mining and Geology, titled "Assessment of Social Vulnerability (SoVI) to Natural Hazards Using Google Earth Engine and Multi-temporal Remote Sensing Data in the Cat Ba Archipelago, Hai Phong City" (Project Code: T25-32). The authors express their sincere appreciation for this support.

References

Abijith, D., Saravanan, S., Parthasarathy, K., Reddy, N. M., Niraimathi, J., Bindajam, A. A., Mallick, J., Alharbi, M. M., & Abdo, H. G. (2025). Assessing the impact of climate and land use change on flood vulnerability: a machine learning approach in coastal region of Tamil Nadu, India. Geoscience Letters, 12(1), 1, https://doi.org/10.1186/s40562-025-00377-7.

Adnyana, I. M., & Wiguna, P. P. K. (2025). Modelling of flood hazard using topographic wetness index in Yeh Ho Watershed, Bali, Indonesia. I In Proceedings of the 10th International

Conference on Sustainable Agriculture, Food, and Energy (SAFE 2024), Jeju, Republic of Korea, 27–29 June 2024; Volume 159, p. 04002, https://doi.org/10.1051/bioconf/202515904002.

Ajtai, I., Ștefănie, H., Maloș, C., Botezan, C., Radovici, A., Bizău-Cârstea, M., & Baciu, C. (2023). Mapping social vulnerability to floods. A comprehensive framework using a vulnerability index approach and PCA analysis. Ecological Indicators, 154, 110838, https://doi.org/10.1016/j.ecolind.2023.110838.

Al-Sababhah, N. M. A. (2023). Integrated Evaluation of Soil Erosion-prone Areas Based on the GIS Technique and the Analytic Hierarchy Process on Hillside Slopes, Northwest of Jordan. Jordan Journal of Earth & Environmental Sciences, 14(2).

Alabbad, Y., & Demir, I. (2025). Understanding flood risk in public transit systems: Insights from accessibility and vulnerability analysis in Iowa. International Journal of Disaster Risk Reduction, 105615, https://doi.org/10.1016/j.ijdrr.2025.105615. (1-20.

Alonso, J. A., & Lamata, M. T. (2006). Consistency in the analytic hierarchy process: a new approach. International journal of uncertainty, fuzziness and knowledge-based systems, 14(04), 445-459, https://doi.org/10.1142/S0218488506004114.

Balaian, S. K., Sanders, B. F., & Abdolhosseini Qomi, M. J. (2024). How urban form impacts flooding. Nature Communications, 15(1), 6911, https://doi.org/10.21203/rs.3.rs-3650683/v1.

Bharwani, S., Taylor, R., Watkiss, P., & Devisscher, T. (2013). Decision Support Methods for Climate Change Adaptation: Analytic Hierarchy Process.

Birkmann, J., Jamshed, A., McMillan, J. M., Feldmeyer, D., Totin, E., Solecki, W., Ibrahim, Z. Z., Roberts, D., Kerr, R. B., & Poertner, H.-O. (2022). Understanding human vulnerability to climate change: A global perspective on index validation for adaptation planning. Science of the Total Environment, 803, 150065, https://doi.org/10.1016/j.scitotenv.2021.150065.

Boateng, I. (2012). GIS assessment of coastal vulnerability to climate change and coastal adaption planning in Vietnam. Journal of Coastal Conservation, 16(1), 25-36, https://doi.org/10.1007/s11852-011-0165-0.

Bukvic, A., Rohat, G., Apotsos, A., & de Sherbinin, A. (2020). A systematic review of coastal vulnerability mapping. Sustainability, 12(7), p. 2822, https://doi.org/10.3390/su12072822.

Chelariu, O.-E., Minea, I., & Iațu, C. (2024). Integrated assessment of geophysical and social vulnerability to natural hazards in North-East Region, Romania. Geomatics, Natural Hazards and Risk, 15(1), 2384607, https://doi.org/10.1080/19475705.2024.2384607.

Cutter, S. L., Boruff, B. J., & Shirley, W. L. (2012). Social vulnerability to environmental hazards. Social Science Quarterly 84, 242–261, https://doi.org/10.1111/1540-6237.8402002.

Dao, M. T., & Dao, M. T. (2024). Assessing the Vulnerability of Phu Quoc Island's Natural and Socioeconomic Systems to Climate Change. IOP Conference Series: Earth and Environmental Science, 1395, 012037, https://doi.org/10.1088/1755-1315/1395/1/012037

De Sherbinin, A., Bukvic, A., Rohat, G., Gall, M., McCusker, B., Preston, B., Apotsos, A., Fish, C., Kienberger, S., & Muhonda, P. (2019). Climate vulnerability mapping: A systematic review and future prospects. Wiley Interdisciplinary Reviews: Climate Change, 10(5), e600, https://doi.org/10.1002/wcc.600.

Du, S., Shi, P., Van Rompaey, A., & Wen, J. (2015). Quantifying the impact of impervious surface location on flood peak discharge in urban areas. Natural Hazards, 76(3), 1457-1471, https://doi.org/10.1007/s11069-014-1463-2.

Giang, P. Q., & Khanal, R. (2024). What next for marine ecosystem management in Vietnam: assessment of coastal economy, climate change, and policy implication. Environmental Research Communications, 6(2), 025002, https://doi.org/10.1088/2515-7620/ad19a5.

Ha-Mim, N. M., & Hossain, M. Z. (2022). Application of GIS and AHP-Based Integrated Methodology for Mapping and Characterizing Socioeconomic Vulnerability to Natural Hazards: A Case Study of Southwestern Coastal Bangladesh. In A System Engineering Approach to Disaster Resilience: Select Proceedings of VCDRR 2021 (pp. 187-203). Springer, https://doi.org/10.1007/978-981-16-7397-9_14.

Hamza, M., Eriksson, K., & Staupe-Delgado, R. (2021). Locating potential sources of capacity and vulnerability in geographically remote areas: Reflections based on three case studies. International Journal of Disaster Risk Reduction, 63, 102433, https://doi.org/10.1016/j.ijdrr.2021.102433.

Hoang, H. T. N., & Truong, H. Q. (2023). Assessing the Impact of Climate Change and the Resilience of Socio-ecological Systems: A Focus on the Red River Delta Biosphere Reserve in Vietnam. In The Vietnam-EU Economic and Trade Forum (pp. 321-342). Singapore: Springer Nature Singapore, https://doi.org/10.1007/978-981-99-8945-4_20.

Hue, L. M., Thao, V. T. P., Vy, N. K., Tra, D. T., & Nam, N. N. (2024). Land cover object change monitoring and environmental suitability confirmation in Cat Ba Biosphere Reserve of Vietnam. Biodiversity, 25(4), 324-336, https://doi.org/10.1080/14888386.2024.2385975.

Ibrahim, M., Huo, A., Ullah, W., Ullah, S., Ahmad, A., & Zhong, F. (2024). Flood vulnerability assessment in the flood prone area of Khyber Pakhtunkhwa, Pakistan. Frontiers in Environmental Science, 12, 1303976, https://doi.org/10.3389/fenvs.2024.1303976

Isia, I., Hadibarata, T., Jusoh, M. N. H., Bhattacharjya, R. K., Shahedan, N. F., Fitriyani, N. L., & Syafrudin, M. (2023). Identifying factors to develop and validate social vulnerability to floods in Malaysia: a systematic review study. Sustainability, 15(17), 12729, https://doi.org/10.3390/su151712729.

Janzen, S., Balzer, J., Merk, F., Eberle, C., Chabi, A., & Walz, Y. (2024). Moving towards a comprehensive evaluation of ecosystem-based disaster risk reduction: The example of agroforestry for flood risk reduction. Nature-Based Solutions, 5, 100104, https://doi.org/10.1016/j.nbsj.2023.100104.

Ji, L., Zhang, L., & Wylie, B. (2009). Analysis of dynamic thresholds for the normalized difference water index. Photogrammetric engineering & remote sensing, 75(11), 1307-1317, https://doi.org/10.14358/PERS.75.11.1307.

Justine, Y. E. D., & Seenath, A. (2025). Vegetative nature-based solutions for coastal flood risk management: Benefits, challenges, and uncertainties. Ocean & Coastal Management, 261, 107520, https://doi.org/10.1016/j.ocecoaman.2024.107520.

Khan, T. U., Nabi, G., Ullah, S., Akbar, A., Omifolaji, J. K., Achakzai, J. K., & Iqbal, A. (2025). Mapping flood resilience: a comprehensive geospatial insight into regional vulnerabilities. Frontiers in Water, 7, 1465505.

Khodaei, H., Nasiri Saleh, F., Nobakht Dalir, A., & Zarei, E. (2025). Future flood susceptibility mapping under climate and land use change. Scientific Reports, 15(1), 12394, https://doi.org/10.3389/frwa.2025.1465505.

Kocsis, I., Bilașco, Ș., Irimuș, I.-A., Dohotar, V., Rusu, R., & Roșca, S. (2022). Flash flood vulnerability mapping based on FFPI using GIS spatial analysis case study: Valea Rea catchment area, Romania. Sensors, 22(9), 3573, https://doi.org/10.3390/s22093573.

Komolafe, A., Awe, B., Olorunfemi, I., & Oguntunde, P. (2020). Modelling flood-prone area and vulnerability using integration of multi-criteria analysis and HAND model in the Ogun River Basin, Nigeria. Hydrological Sciences Journal, 65(10), 1766-1783, https://doi.org/10.1080/02626667.2020.1764960.

Konapala, G., Kumar, S. V., & Ahmad, S. K. (2021). Exploring Sentinel-1 and Sentinel-2 diversity for flood inundation mapping using deep learning. ISPRS Journal of Photogrammetry and Remote Sensing, 180, 163-173, https://doi.org/10.1016/j.isprsjprs.2021.08.016.

Ma, J., & Mostafavi, A. (2024). Urban form and structure explain variability in spatial inequality of property flood risk among US counties. Communications Earth & Environment, 5(1), 172, https://doi.org/10.1038/s43247-024-01337-3.

Mai, N. T., & Truong, D. D. (2022). Farming Households' Perception on Natural Disaster Impacts to Livelihoods and Adaptation Practices: A Case Study of Coastal Provinces in Central Vietnam. International Journal of Sustainable Development & Planning, 17(2), https://doi.org/10.18280/ijsdp.170223.

Maliva, R. (2021). Climate change and small islands. In Climate Change and Groundwater: Planning and Adaptations for a Changing and Uncertain Future: WSP Methods in Water Resources Evaluation Series No. 6 (pp. 155-176). Springer.

Miranda, F., Franco, A. B., Rezende, O., da Costa, B. B., Najjar, M., Haddad, A. N., & Miguez, M. (2023). A GIS-based index of physical susceptibility to flooding as a tool for flood risk management. Land, 12(7), 1408, https://doi.org/10.3390/land12071408.

Newspaper, H. P. (2025). Flood alert issued for low-lying areas in Hai Phong due to rising river levels. Retrieved 19/11/2025 from https://dangcongsan.vn/haiphong/tin-tuc-hoat-dong/canh-bao-lu-tren-cac-song-o-hai-phong.html?utm_source=chatgpt.com

Oroud, I. M. (2025). The Relative Impact of Urbanization Expansion and Climate Change on Flood Hazard in Amman City. Jordan Journal of Earth & Environmental Sciences, 16(1).

Parmesan, C., Morecroft, M. D., & Trisurat, Y. (2022). Terrestrial and Freshwater Ecosystems and Their Services. In: Climate Change 2022: Impacts, Adaptation and Vulnerability. Contribution of Working Group II to the Sixth Assessment Report of the Intergovernmental Panel on Climate Change [H.-O. Pörtner, D.C. Roberts, M. Tignor, E.S. Poloczanska, K. Mintenbeck, A. Alegría, M. Craig, S. Langsdorf, S. Löschke, V. Möller, A. Okem, B. Rama (eds.)]. Cambridge University Press, Cambridge, UK and New York, NY, USA, pp. 197–377, doi:10.1017/9781009325844.004.

Rautela, K. S., Kumar, D., Gandhi, B. B. G. R., Kumar, A., & Dubey, A. K. (2023). Flood Vulnerability Assessment Across Alaknanda River Basin using GIS-based combined analysis of geomorphometric approach and MCDM-AHP. Journal of the Geological Society of India, 99(11), 1604-1615, https://doi.org/10.1007/s12594-023-2512-9.

Rudin, C. (2019). Stop explaining black box machine learning models for high stakes decisions and use interpretable models instead. Nature machine intelligence, 1(5), 206-215, https://doi.org/10.1038/s42256-019-0048-x.

Saaty, T. (1980). McGraw-Hill; New York: 1980. The Analytic Hierarchy Process: Planning, Priority Setting, Resource Allocation McGraw-Hill, New York, 1980.

Shivhare, V., Kumar, A., Kumar, R., Shashtri, S., Mallick, J., & Singh, C. K. (2024). Flood susceptibility and flood frequency modeling for lower Kosi Basin, India using AHP and Sentinel-1 SAR data in geospatial environment. Natural Hazards, 120(13), 11579-11610, https://doi.org/10.1007/s11069-024-06614-0

Son, C. H., Lee, C. H., & Ban, Y. U. (2023). Analysis of the impact and moderating effect of high-density development on urban flooding. Heliyon, 9(12), https://doi.org/10.1016/j.heliyon.2023.e22695

Ta, K. L., & Linh, P. K. (2024). Integrating Women's Rights and Climate Migrant Protection: Bridging Gaps in Vietnam. Human Rights in the Global South (HRGS), 3(1), 79-100, https://doi.org/10.56784/hrgs.v3i2.109

Tariq, A., Yan, J., Ghaffar, B., Qin, S., Mousa, B., Sharifi, A., Huq, M. E., & Aslam, M. (2022). Flash flood susceptibility assessment and zonation by integrating analytic hierarchy process and frequency ratio model with diverse spatial data. Water, 14(19), 3069, https://doi.org/10.3390/w14193069.

Tetteh, A. T., Moomen, A.-W., Yevugah, L. L., & Tengnibuor, A. (2024). Geospatial approach to pluvial flood-risk and vulnerability assessment in Sunyani Municipality. Heliyon, 10(18).

Tuyet Hanh, T. T., Huong, L. T. T., Huong, N. T. L., Linh, T. N. Q., Quyen, N. H., Nhung, N. T. T., Ebi, K., Cuong, N. D., Van Nhu, H., & Kien, T. M. (2020). Vietnam climate change and health vulnerability and adaptation assessment, 2018. Environmental Health Insights, 14, 1178630220924658.

Uddameri, V., & Hernandez, E. A. (2025). Machine Learning for Flood Resiliency—Current Status and Unexplored Directions. Environments, 12(8), 259, https://doi.org/10.3390/environments12080259.

Udie, J., Bhattacharyya, S., & Ozawa-Meida, L. (2018). A conceptual framework for vulnerability assessment of climate change impact on critical oil and gas infrastructure in the niger delta. Climate, 6(1), 11, https://doi.org/10.3390/cli6010011

Van Phong, T., Nguyen, D. D., & Pham, B. T. (2023). Modeling and Mapping of Flood Susceptibility at Que Son District, Quang Nam Province, Vietnam using CatBoost. IOP conference series: materials science and engineering (Vol. 1289, No. 1, p. 012019). IOP Publishing, 10.1088/1757-899X/1289/1/012019.

Van Quan, N., Duc, T. T., & Van Huy, D. (2010). Landscapes and ecosystems of tropical limestone: case study of the Cat Ba Islands, Vietnam. Journal of Ecology and Environment, 33(1), 23-36, http://dx.doi.org/10.5141/JEFB.2010.33.1.023.

VnExpress. (2024). Cat Ba tourist island ravaged by Typhoon Yagi. Retrieved 19/11/2025 from https://e.vnexpress.net/photo/places/cat-ba-tourist-island-ravaged-by-typhoon-yagi-4791507.html?utm_source=chatgpt.com

Vousdoukas, M. I., Athanasiou, P., Giardino, A., Mentaschi, L., Stocchino, A., Kopp, R. E., Menéndez, P., Beck, M. W., Ranasinghe, R., & Feyen, L. (2023). Small Island Developing States under threat by rising seas even in a 1.5 C warming world. Nature sustainability, 6(12), 1552-1564, https://doi.org/10.1038/s41893-023-01230-5

Xie, W., & Meng, Q. (2023). An integrated PCA–AHP method to assess urban social vulnerability to sea level rise risks in Tampa, Florida. Sustainability, 15(3), 2400, https://doi.org/10.3390/su15032400

Yarveysi, F., Alipour, A., Moftakhari, H., Jafarzadegan, K., & Moradkhani, H. (2023). Block-level vulnerability assessment reveals disproportionate impacts of natural hazards across the conterminous United States. Nature Communications, 14(1), 4222, https://doi.org/10.1038/s41467-023-39853-z.

Zakir, H. M. (2024). Study on the groyne arrangement for protection of riverbank erosion of braided river in lowland area. Doctoral dissertation). Nagoya University.

Zhran, M., Ghanem, K., Tariq, A., Alshehri, F., Jin, S., Das, J., Pande, C. B., Pramanik, M., Hasher, F. F. B., & Mousa, A. (2024). Exploring a GIS-based analytic hierarchy process for spatial flood risk assessment in Egypt: A case study of the Damietta branch. Environmental Sciences Europe, 36(1), 184, https://doi.org/10.1186/s12302-024-01001-9.